Inorganic Chemistry Research

Article

Theoretical and Experimental Investigation of Reaction Between a Cycloplatinated(II) Complex Containing Pyridine Ligand with Acyl Chloride

Fatemeh Niroomand Hosseini*

Department of Chemistry, Shiraz Branch, Islamic Azad University, Shiraz 71993–37635, Iran

Received: December 18, 2022; Accepted: January 2, 2023

Cite This: *Inorg. Chem. Res.* **2022**, *6*, 114-118. DOI: 10.22036/icr.2023.377317.1139

Abstract: The reaction of cycloplatinated(II) complex [PtMe(bhq)(py)], **1**, (bhqH = benzo[h]quinoline and py = pyridine) with acyl chloride gives the organoplatinum(IV) complex [PtCl(COMe)Me(bhq)(py)], **POX**. Attempts to grow crystals of the Pt(IV) complex **POX** in CH_2Cl_2 solvent forms the trichloro cycloplatinated(IV) complex [$PtCl_3$(bhq)(py)], $\mathbf{P_{cryst}}$, which its structure is determined by X-ray crystallography. The mechanism of the reactions is computationally investigated which suggest that first C-Cl bond of acyl chloride is oxidatively added to Pt(II) center of complex **1** through a cationic five-coordinate intermediate to give an octahedral Pt(IV) complex in which two new bonds, Pt-Cl and Pt-C(O)Me, are formed. In the resulted Pt(IV) complex, two Pt-Me and Pt-C(O)Me bonds are in the cis position to each other which increase the possibility of C-C reductive elimination. The energy barriers for both these two elementary reactions and structures are calculated using DFT calculations.

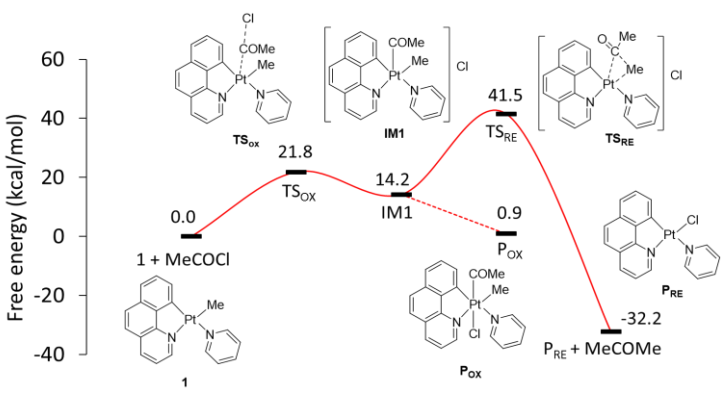

Keywords: Platinum, Oxidative addition, Reductive elimination, DFT Calculation, Mechanisms

1. INTRODUCTION

Two elementary reactions, i.e. oxidative addition and reductive elimination, are among the most important reactions in organometallic chemistry and organic synthesis due to their essential role for completing the catalytic processes.[1-4] There are many reports in the literature including platinum(II) complexes in which these complexes have been extensively used to study their chemistry.[5-9] Chelating N^N donor (such as 1,10-phenanthroline) organoplatinum complexes have been used in this regard.[10,11] These organoplatinum(II) complexes bearing N^N chelating ligands are extremely reactive toward oxidative addition reactions, and in the most cases, it is confirmed that they proceed through an S_N2 mechanism.[12,13] On the other hand, cycloplatinated complexes in which C^N chelate ligands are 2-phenypyridinate or benzo-h-quinolate, have been recently used in oxidative addition and reductive elimination process, although compared to N^N complexes less studies have been reported on the reactivity of these cyclometalated compounds.[12,14-16] The attractive chemistry of the cyclometalated compounds and importance of their reactivity prompted us to investigate the reactivity of cycloplatinated (II) complex [PtMe(bhq)(py)], **1**, in which bhqH = benzo[h]quinoline and py = pyridine, in acyl chloride oxidative addition to Pt center to form cycloplatinated(IV) complex [PtCl(COMe)Me(bhq)(py)], **POX**. Then, C–C bond forming reductive elimination from **POX** is computationally investigated to give [PtCl(bhq)(py)], **PRE**. DFT calculations are also used to give further insight into the possible transition states and intermediates during these processes, i.e. C–Cl bond oxidative addition and C–C reductive elimination.

2. RESULTS AND DISCUSSION

The starting Pt(II) complex [PtMe(bhq)(py)], **1**, reacts with acyl chloride to produce the cycloplatinated(IV) complex [PtCl(COMe)Me(bhq)(py)], **POX**. As shown in Figure 1, the ^{1}H NMR spectrum of **POX** shows two singlet signals at 1.18 ($^2J_{PtH}$ = 71.6 Hz) and 2.73 ($^3J_{PtH}$ = 11.0 Hz) for protons of Me and COMe groups, respectively. The coupling constant value of $^2J_{PtH}$ = 71.6 Hz for Pt-Me is much lower than the corresponding value of 85.4 Hz for Me found for the starting Pt(II) complex **1**, showing the oxidation of Pt(II) complex **1** to Pt(IV) complex **POX**.

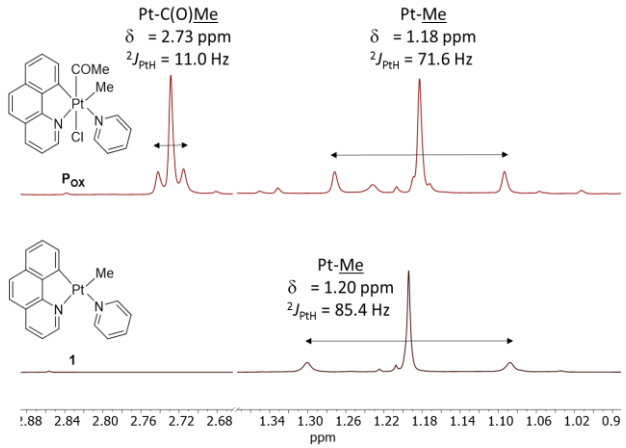

Fig. 1. ^{1}H NMR spectra (aliphatic region) of the starting Pt(II) complex **1** and Pt(IV) product $\mathbf{P_{OX}}$ (resulting from the oxidative addition of complex 1 and acyl chloride in $CDCl_3$. The assignments and coupling constants are shown.

Attempts to grow suitable crystals of cyclometalated Pt(IV) complex [PtCl(COMe)Me(bhq)(py)], $\mathbf{P_{OX}}$, for a single crystal X-ray diffraction experiment in solvents such as acetone and benzene were not successful. During the crystallization process in CH_2Cl_2 at room temperature, an interesting trichloro Pt(IV) complex [$PtCl_3$(bhq)(py)], $\mathbf{P_{cryst}}$, is obtained. As suggested in Scheme 1, the formation of this complex can proceed via C–C bond reductive elimination from $\mathbf{P_{OX}}$ to give [PtCl(bhq)(py)], $\mathbf{P_{RE}}$ (see the Computational section). The reaction of CH_2Cl_2 solvent with $\mathbf{P_{RE}}$ forms the final product $\mathbf{P_{cryst}}$.

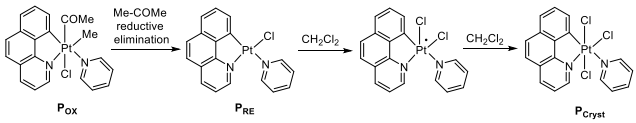

Scheme 1. Suggested route for formation of complex $\mathbf{P_{cryst}}$ from $\mathbf{P_{OX}}$ in CH_2Cl_2 solvent during crystallization process.

The solid state structure of complex $\mathbf{P_{cryst}}$ was further determined crystallographically as shown in Figure 2. The crystallographic data and structural analysis are given in Table 1 and selected bond distances and angles with estimated standard deviations are reported in Table 2. It crystallizes in the Triclinic crystal system in the space group P-1. The complex $\mathbf{P_{cryst}}$ has an octahedral geometry with PtCN2Cl3 coordination, in which the N atom of the bhq ligand is trans to the N atom of the pyridine. The maximum deviation from the ideal geometry in both molecules is found for the chelating bite angle of the bhq ligand, i.e. C(16)-Pt(1)-N(2) = 81.8(2)°, which indicates that the bhq chelate is probably under strain. The Pt-Cl(3) bond is longer than Pt-Cl(1) and Pt-Cl(2), which is due to higher trans influence of carbon compare to Cl.

Table 1. Crystal data and structure refinement for complex $\mathbf{P_{cryst}}$

Empirical formula	$C_{18}H_{13}Cl_3N_2Pt$
Formula weight	558.74
Temperature, K	100(2)
Wavelength, Å	0.71073
Crystal system	Triclinic
Space group	P-1
Unit cell dimensions	a = 7.968(3) Å b = 8.334(3) Å c = 12.640(4) Å α= 94.564(9)° β = 93.339(3)° γ = 99.949(11)°
Volume	6246.0(16) Å^3
Z	2
Density (calculated)	2.253 g-cm^{-3}
Absorption coefficient	9.005 mm^{-1}
F(000)	528
Theta range for data collection	1.617 to 27.312°
Reflections collected	5278
Independent reflections	3530 [R(int) = 0.0283]
Completeness to theta = 25.242°	97.1 %
Absorption correction	Semi-empirical from equivalents
Refinement method	F^2
Data / restraints / parameters	3530 / 0 / 217
Goodness-of-fit on F^2	0.995
Final R indices [$I > 2\sigma$ (I)]	R1 = 0.0341, wR2 = 0.0637
R indices (all data)	R1 = 0.0471, wR2 = 0.0681
Largest diff. peak and hole	1.131 and -0.805-Å^{-3}

Table 2. Selected experimental bond distances (Å) and angles (deg) for complex $\mathbf{P_{cryst}}$

bond distance or angle		bond angle	
Cl(1)-Pt(1)	2.3134(19)	N(2)-Pt(1)-Cl(1)	88.84(16)
Cl(2)-Pt(1)	2.3200(18)	N(1)-Pt(1)-Cl(1)	90.05(15)
Cl(3)-Pt(1)	2.4339(16)	C(16)-Pt(1)-Cl(2)	89.17(18)
N(1)-Pt(1)	2.047(5)	N(2)-Pt(1)-Cl(2)	88.71(16)
N(2)-Pt(1)	2.037(5)	N(1)-Pt(1)-Cl(2)	92.38(15)
C(16)-Pt(1)	2.021(6)	Cl(1)-Pt(1)-Cl(2)	177.47(5)
C(16)-Pt(1)-N(2)	81.8(2)	C(16)-Pt(1)-Cl(3)	175.04(16)
C(16)-Pt(1)-N(1)	96.1(2)	N(2)-Pt(1)-Cl(3)	93.39(14)
N(2)-Pt(1)-N(1)	177.6(2)	N(1)-Pt(1)-Cl(3)	88.66(14)
C(16)-Pt(1)-Cl(1)	89.86(18)	Cl(1)-Pt(1)-Cl(3)	88.73(6)

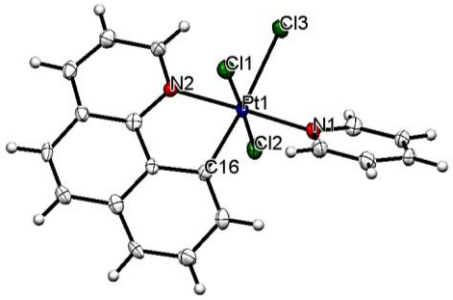

Figure 2. Perspective view of the complex [$PtCl_3$(bhq)(py)], $\mathbf{P_{cryst}}$, together with the numbering scheme. Ellipsoids are drawn at the 50% probability level. Selected bond distances and angles are shown in Table 2.

Mechanistic study of the oxidative addition process

It is commonly established that alkyl halide and other small organic reagents such as acyl halides, are

oxidatively added to d^8 square planar complexes via an S_N2 mechanism.[12,13] This process includes nucleophilic substitution of halide by metal complex to give a metal–carbon bond, followed by coordination of halide to vacant site of 5-coordinate square pyramidal intermediate to give a six-coordinate octahedral product. The oxidative addition reactions, (**1** → **Pox**) shown in Scheme 2, are computationally investigated and possible transition states and intermediates along with energy barrier needed for the reaction are computed.

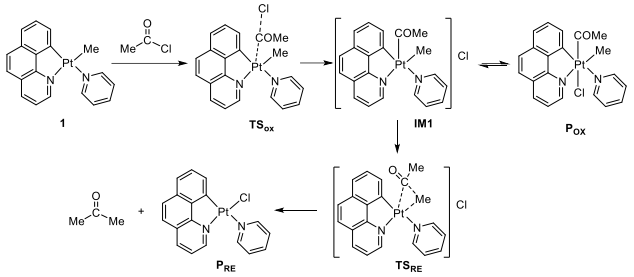

Scheme 2. Schematic illustrating oxidation addition of complex **1** with acyl chloride and C-C reductive elimination from Pt(IV) product.

The DFT-optimized structures of the reactants, transition states, intermediates and products for the reaction of **1** with acyl chloride at the B3LYP level are illustrated in Figure 3. Some important geometrical parameters are also reported.

Three steps can be proposed for oxidative addition process **1** → **Pox** (see Scheme 2).

Step 1. As shown in Scheme 1, two reactants at the beginning are unbounded. The rate-controlling step includes the nucleophilic substitution of chloride in acyl chloride by the Pt center of **1**. Upon the substitution of chloride and the simultaneous partial removal of chloride ion, the transition state **TSox** is formed. The **TSox** structure includes the Cl-C_{acyl}-Pt, Pt-C_{acyl}-Me and Pt-C_{acyl}-O arrangements with bond angles of 97.1, 103.1 and 105.8°, respectively. During the formation of **TSox** in the first step, the major changes in bond lengths are seen for Cl-C_{acyl} and Pt-C_{acyl} bonds. The Cl···C_{acyl} distance increases from 1.922 Å in acyl chloride to 2.176 Å in transition structure **TSox**, while the Pt···C_{acyl} distance decreases from far apart in the reactants to 2.572 Å in **TSox**. As shown in Figure 3, no significant changes were observed for the other bonds, showing that the oxidative addition reaction of acyl chloride to complex **1** contains concurrently the breaking of Cl-C_{acyl} bond and the construction of the Pt-C_{acyl} bond in **TSox**. The observation of a negative imaginary frequency confirms the accuracy of transition state, **TSox**. This frequency corresponds to a Cl-C_{acyl}-Pt stretching vibrational mode.

Step 2. The formation of **TSox** is followed by fully breaking and forming of Cl-C_{acyl} and Pt-C_{acyl} bonds, respectively, to give the ionic 5-coordinate $[PtMe(COMe)(bhq)(py)]^+Cl^-$ intermediate, **IM1**. The cationic part of this intermediate has a square pyramidal geometry, where the acyl group is located in the apical position. The chloride ion is in the outer sphere of Pt complex.

Step 3. At the end, the free chloride ion coordinates to the Pt(IV) center of **IM1** to give the acylplatinum(IV) product of [PtMeCl(COMe)(bhq)(py)], **Pox**, with an octahedral geometry around the Pt center (see Figure 3). The Pt-Cl and Pt–C_{acyl} bond lengths in **Pox** are 2.660 and 2.054 Å, respectively. As clear in Figure 3, the bond lengths of the reactant **1** (with the Pt center in oxidation state +2) are shorter than those of the corresponding Pt(IV) product, **Pox**. For example, the Pt–C_{Me} bond in **1** is shorter (2.063 Å) than that in **Pox** (2.080 Å).

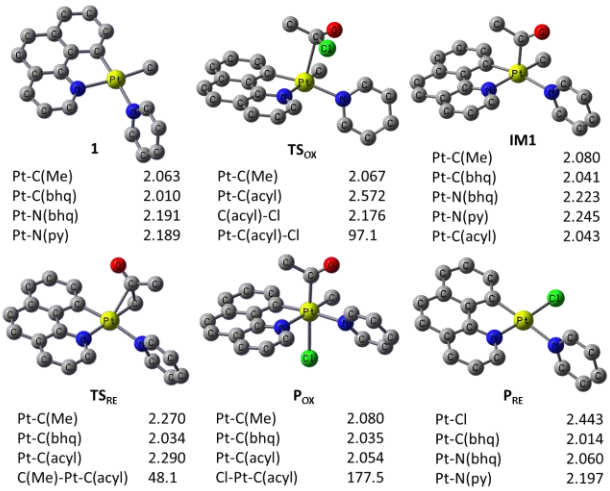

Figure 3. Optimized structures of the Pt species involved in the reaction of complex **1** with acyl chloride. Some important geometrical parameters (Å and °) are also shown.

Mechanistic study of the reductive elimination process

It is well recognized that the C-C reductive elimination from the saturated d^6 6-coordinate complexes such as Pt(IV) complexes usually take places through prior dissociation of a ligand.[10] Indeed, the formation of a cationic five-coordinated intermediate is responsible for the C-C reductive elimination process.[17-19] Also, the C–C reductive elimination from 5-coordinate d^6 metal complexes occurs more easily than from the corresponding 6-coordinate complexes.[20] To investigate the C-C coupling reductive elimination from cycloplatinated(IV) complex **Pox**, we computed acetone elimination from **Pox** to give [PtMe(bhq)(py)], **1**, (see Scheme 2). The acetone reductive elimination from intermediate **IM1** proceeds through transition state **TSRE**, (see Scheme 2) in which the bonds between Pt center and Me and acyl leaving groups (Me-C(O)Me) are extended (from 2.080 and 2.043 Å in **IM1** to 2.270 and 2.290 Å in

TS$_{RE}$, respectively) and the Me-Pt-acyl bond angle is considerably reduced (from 88.6° in **IM1** to 48.1° in **TS$_{RE}$**). As acetone dissociates, the Pt(II)-Cl bond is formed giving [PtCl(bhq)(py)] complex, **P$_{RE}$**.

Free energy change profile

The free energy profile for the reaction of complex **1** with acyl chloride is shown in Figure 4. The formation of intermediate **IM1** can be considered as the first step of oxidative addition of MeCOCl to complex **1**. This step proceeds through **TS$_{OX}$** with the energy barrier of 21.8 kcal/mol. Trapping of 5-coordinated intermediate **IM1** by chloride ion is a downhill process to form the cycloplatinated(IV) product **P$_{OX}$**, which is located 13.3 kcal/mol lower in energy compare to **IM1**.

The cycloplatinated(II) product **P$_{RE}$** resulted from the C−C reductive elimination in **IM1** via the transition state **TS$_{RE}$** (Scheme 2 and Figure 4). To access **TS$_{RE}$** from **IM1** (which is +14.2 kcal/mol higher in energy than **1**), an additional input of +27.3 kcal/mol is required. As Me−COMe dissociates, the Pt(II)-Cl bond is formed, giving the final reductive elimination product **P$_{RE}$**. The Pt(II) product **P$_{RE}$** is calculated to be more stable than **1** and **P$_{OX}$** by 32.2 and 33.1 kcal/mol, respectively.

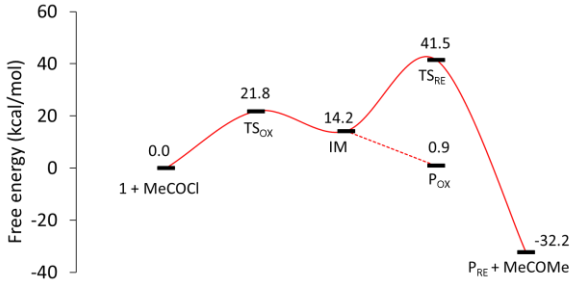

Figure 4. Computed energy profile for oxidative addition of acyl chloride to the platinum(II) complex **1** and C-C reductive elimination from platinum(IV) complex.

3. CONCLUSIONS

The experimental study of the oxidation of cycloplatinated(II) complex [PtMe(bhq)(py)], **1**, by acyl chloride showed that the C-Cl bond can be activated by Pt(II) center to form cycloplatinated(IV) complex [PtCl(COMe)Me(bhq)(py)], **P$_{OX}$**, with two new bonds, Pt-Cl and Pt-C$_{acyl}$. Attempts to grow crystals of **P$_{OX}$** in CH_2Cl_2 solvent forms the trichloro cycloplatinated(IV) complex [$PtCl_3$(bhq)(py)], **P$_{cryst}$**, which its structure is determined by X-ray crystallography. The theoretical studies in the present work focus on the C-Cl oxidative addition reaction of **1** with CH_3COCl by using B3LYP calculations. The reaction proceeds by an S_N2 reaction mechanism via a transition state with a bent arrangement of the Cl-C$_{acyl}$-Pt moiety. The intermediate of the reaction is an ionic complex [PtMe(COMe)(bhq)(py)]$^+$Cl$^-$ with the chloride remaining in the outer coordination sphere. The values of the calculated free energies of activation in acetone was found to be 21.8 kcal/mol. The C-C reductive elimination from [PtCl(COMe)Me(bhq)(py)], **P$_{OX}$**, to give [PtCl(bhq)(py)], **P$_{RE}$**, proceeds through a three-centred trigonal bipyramidal transition state, with the free energy of activations being 41.5 kcal/mol.

4. EXPERIMENTAL AND COMPUTATIONAL DETAILS

^{1}H NMR spectra were recorded on a Brucker 400 MHz spectrometer in $CDCl_3$ as solvent and referenced to external TMS (0.00 ppm). All chemical shifts and coupling constants are given in ppm and Hz, respectively. Melting points were recorded on a Buchi 530 apparatus. [PtMe(bhq)(py)], **1**, was prepared as reported previously.[21]

[PtCl(COMe)Me(bhq)(py)], **P$_{OX}$**. An excess of acyl chloride (50 µL) was added to a solution of complex **1**, (40 mg) in 25 mL of acetone at room temperature. The mixture was allowed to stand at this condition for 1 h, and then the solvent was removed under reduced pressure. The residue was washed twice with ether, and the product was dried under vacuum. Yield: 65%, mp = 217 °C (decomp). ^{1}H NMR data: δ 1.18 [s, 3H, $^2J_{PtH}$ = 71.6 Hz, Me ligand], 2.73 (s, 3H, $^3J_{PtH}$ = 11.0, COMe)], 7.10-8.95 [protons of bhq and py ligand].

Crystallography details

Single crystal X-ray diffraction data for complex **P$_{cryst}$** were collected on a Bruker KAPPA APEX II diffractometer equipped with an APEX II CCD detector using a TRIUMPH monochromator with a Mo Kα X-ray source (λ = 0.71073 Å). The crystal was mounted on a cryoloop under Paratone-N oil and kept under nitrogen. Absorption correction of the data was carried out using the multiscan method SADABS.[22] Subsequent calculations were carried out using SHELXTL.[23] Structure determination was done using intrinsic methods. Structure solution, refinement, and creation of publication data was performed using SHELXTL. Crystallographic data is presented in Table 1. Crystallographic data for the structural analysis have been deposited with the Cambridge Crystallographic Data Centre, CCDC 2233679. Copies of this information may be obtained free of charge from: The Director, CCDC, 12 Union Road, Cambridge, CB2 1EZ, UK. Fax: +44(1223)336-033, e-mail: deposit@ccdc.cam.ac.uk, or via the web at www.ccdc.cam.ac.uk.

Computational details

Gaussian 09[24] was used to fully optimize all the structures at the B3LYP level of density functional theory. The starting structures were created by the GaussView program and optimized using the CPCM solvation method,[25] considering acetone as the solvent as implemented in the Gaussian program. The effective core potential of Hay and Wadt with a double-ξ valence basis set (LANL2DZ) was chosen to describe Pt and Cl.[26] The 6-311G(d) basis set was used for other atoms. Frequency calculations were carried out at the same level of theory to identify whether the calculated stationary point is a minimum (zero imaginary frequency) or a transition structure (one imaginary frequency).

CONFLICTS OF INTEREST

The author declares no conflict of interest.

ACKNOWLEDGMENTS

Support from the Islamic Azad University (Shiraz Branch) is appreciated.

AUTHOR INFORMATION

Corresponding Author

Fatemeh Niroomand Hosseini: Email: fniroomand55@yahoo.com, *ORCID*: 0000-0002-5856-8104.

REFERENCES

1. T. Chu and G. I. Nikonov, *Chem. Rev.*, 2018, **118**, 3608-3680.
2. D. Bacciu, K. J. Cavell, I. A. Fallis and L. l. Ooi, *Angew. Chem. Int. Ed.*, 2005, **44**, 5282-5284.
3. A. L. Smith, K. I. Hardcastle and J. D. Soper, *J. Am. Chem. Soc.*, 2010, **132**, 14358-14360.
4. A. Behnia, M. A. Fard, J. M. Blacquiere and R. J. Puddephatt, *Organometallics*, 2020, **39**, 4037-4050.
5. C. M. Anderson, G. Brown, M. W. Greenberg, D. Yu, N. Bowen, R. Ahmed, M. Yost-Bido and A. Wray, *Tet. Lett.*, 2019, **60**, 151156.
6. H. R. Shahsavari, R. Babadi Aghakhanpour, A. Biglari, M. Niazi, P. Mastrorilli, S. Todisco, V. Gallo, E. Lalinde, M. T. Moreno and N. Gimenez, *Organometallics*, 2020, **39**, 417-424.
7. M. Bavi, S. M. Nabavizadeh, F. N. Hosseini, F. Niknam, P. Hamidizadeh, S. J. Hoseini, F. Raoof and M. M. Abu-Omar, *ACS Omega*, 2020, **5**, 28621-28631.
8. S. M. Nabavizadeh, H. Molaee, E. Haddadi, F. N. Hosseini, S. J. Hoseini and M. M. Abu-Omar, *Dalton Trans.*, 2021, **50**, 15015-15026.
9. A. J. Canty, A. Ariafard and S. M. Nabavizadeh, *Inorg. Chem. Res.*, 2022, **6**, 93-97.
10. F. Niroomand Hosseini, S. M. Nabavizadeh, R. Shoara, M. Dadkhah Aseman and M. M. Abu-Omar, *Organometallics*, 2021, **40**, 2051-2063.
11. M. A. Fard and R. J. Puddephatt, *J. Organomet. Chem.*, 2020, **910**, 121139.
12. M. Crespo, M. Martinez, S. M. Nabavizadeh and M. Rashidi, *Coord. Chem. Rev.*, 2014, **279**, 115-140.
13. L. M. Rendina and R. J. Puddephatt, *Chem. Rev.*, 1997, **97**, 1735-1754.
14. M. Dadkhah Aseman, M. Nikravesh, A. Abbasi and H. R. Shahsavari, *Inorg. Chem.*, 2021, **60**, 18822-18831.
15. Z. Farasat, S. M. Nabavizadeh, F. Niroomand Hosseini, S. J. Hoseini and M. M. Abu-Omar, *Inorg. Chem.*, 2021, **60**, 1998-2008.
16. G. Aullón, M. Crespo, J. Jover and M. Martínez, in *Adv. Inorg. Chem.*, Elsevier, 2017, vol. 70, pp. 195-242.
17. M. G. Haghighi, S. M. Nabavizadeh, M. Rashidi and M. Kubicki, *Dalton Trans.*, 2013, **42**, 13369-13380.
18. J. Procelewska, A. Zahl, G. Liehr, R. Van Eldik, N. A. Smythe, B. S. Williams and K. I. Goldberg, *Inorg. Chem.*, 2005, **44**, 7732-7742.
19. D. M. Crumpton and K. I. Goldberg, *J. Am. Chem. Soc.*, 2000, **122**, 962-963.
20. M. Safa and R. J. Puddephatt, *J. Organomet. Chem.*, 2013, **724**, 7-16.
21. N. H. Fatemeh, Z. Farasat, S. M. Nabavizadeh, G. Wu and M. M. Abu-Omar, *J. Organomet. Chem.*, 2019, **880**, 232-240.
22. G. Sheldrick, *SADABS, Empirical Absorption Correction Program; University of Göttingen: Germany, 1997*, 2005.
23. SHELXTL PC, Version 6.12, Bruker AXS Inc., Madison, WI, 2005.
24. M. Frisch, G. Trucks, H. B. Schlegel, G. Scuseria, M. Robb, J. Cheeseman, G. Scalmani, V. Barone, B. Mennucci and G. Petersson, Gaussian 09, revision D. 01, Gaussian, Inc., Wallingford CT.
25. M. Cossi, N. Rega, G. Scalmani and V. Barone, *J. Comput. Chem.*, 2003, **24**, 669-681.
26. P. J. Hay and W. R. Wadt, *J. Chem. Phys.*, 1985, **82**, 270-283.